3D nonlinear seismic analysis and design of base-isolated buildings under near field ground motions

Authors:

Mohammed Tamahloult, PhD student
Laboratory of Earthquake Engineering
and Structural Dynamics
Ecole Nationale Polytechnique, Algeria
Department of Civil Engineering
mohammed.tamahloult@g.enp.edu.dz

Prof. **Boualem Tiliouine**, PhD. CE
Laboratory of Earthquake Engineering
and Structural Dynamics
Ecole Nationale Polytechnique, Algeria
Department of Civil Engineering
boualem.tiliouine@g.enp.edu.dz
Corresponding author

Professional paper

Mohammed Tamahloult, Boualem Tiliouine

3D nonlinear seismic analysis and design of base-isolated buildings under near field ground motions

The structural performance of base-isolated buildings during past earthquakes confirmed the suitability of Lead Rubber Bearing (LRB) isolators. To assess the effectiveness of such isolators, 3D base-fixed and associated base-isolated models of a multi-story building are performed for three components recorded at each of the three stations with the closest distances to the seismic fault of approximately 5.54, 11.39, and 17.82 km during the 6.7 Mw Northridge earthquake in 1994. In this study, we discuss important issues regarding the analysis and design of base-isolated buildings under near-field ground motions at both the Design Basis Earthquake (DBE) and Maximum Capable Earthquake (MCE) levels. The results demonstrate that although the shear strain and stability conditions are fulfilled, it is crucial to satisfy the rollout condition requirements because of the large isolator displacement at MCE level while utilising supplemental viscous dampers to improve the desired efficiency of isolation.

Key words:

near field ground motions, base-isolated buildings, 3D nonlinear earthquake response, LRB isolators, seismic design, stability checks

Stručni rad

Mohammed Tamahloult, Boualem Tiliouine

3D nelinearna seizmička analiza i projektiranje izoliranih zgrada pri gibanjima tla s plitkim žarištem

Učinkovitost izoliranih zgrada tijekom prošlih potresa potvrdio je prikladnost izolatora od gumenog ležišta s olovnom jezgrom (LRB). Kako bi se procijenila učinkovitost takvih izolatora, za tri komponente snimljene tijekom potresa u Northridgeu 1994. godine, na trima postajama s udaljenostima od seizmičkog rasjeda na 5.54, 11.39, 17.82 i 6.7 Mw , razvijeni su 3D modeli višekatne zgrade s fiksnom bazom i modeli s pridruženom izoliranom bazom. U ovom se radu dotičemo važnih pitanja u vezi s analizom i projektiranjem izoliranih zgrada pod utjecajem gibanja tla s plitkim žarištem pri razinama predviđenog potresa (engl. *Design Basis Earthquake* - DBE) i najjačega mogućeg potresa (engl. Maximum Capable Earthquake - MCE). Rezultati pokazuju da, iako su uvjeti posmične deformacije i stabilnosti ispunjeni, ključno je zadovoljiti zahtjeve uvjeta izvlačenja (engl. rollout) zbog velikog pomaka izolatora na razini MCE uz korištenje dodatnih viskoznih prigušivača za poboljšanje željene učinkovitosti izolacije.

Ključne riječi:

gibanja tla s plitkim žarištem, izolirane zgrade, 3D nelinearni odgovor na potres, LRB izolatori, seizmička konstrukcija, provjere stabilnosti

1. Introduction

The structural performance of base-isolated structures during past earthquakes confirmed the suitability of Lead Rubber Bearings (*LRBs*) as effective base isolators. In fact, structures such as residential buildings incorporing LRBs performed significantly better than base-fixed buildings during the near-field 1994 Northridge and 1995 Kobe earthquakes, confirming their suitability as effective seismic base isolators in near-field regions [1, 2]. Seismic ground motions recorded near the source of rupture have different characteristics than far field ground motions and significantly differ in their influence on the inelastic response of multi-story buildings [3, 4]. Also, near-fault modification factors that are relatively comparable to those of UBC97, Chinese, and Taiwanese seismic design codes for short and long periods structures have been proposed [5].

Laminated rubber bearings, Friction Pendulum System, and Teflon-Steel friction bearings are some of the commonly adopted systems for seismic base isolation. Furthermore, they are comparable to other isolation devices and are known for their longevity, economy, and better control over their properties [6]. They can support heavy weights because of their structural rigidity in a vertical direction. However, they are horizontally very flexible allowing the superstructures to move almost in rigid body motion during earthquake ground motions [7]. The Uniform Building Code (*UBC97*) [8] predicts that the superstructures of base-isolated buildings will behave practically elastically under the design basis earthquake *(DBE)* contrary to the case under the Maximum Capable Earthquake *(MCE)* level. LRBs are formed by inserting a lead core into laminated elastomeric bearings and are capable of providing high damping and initial rigidity. A bilinear model is used to depict the mechanical properties of the lead-plug bearing [9, 10].

Alhan and Öncü-Davas [11] proposed a methodology that can appropriately identify the optimum criteria of the isolation system, including the isolation period and the characteristic force ratio, necessary to fulfil a performance target in the near-field region.

According to Mayes and Naeim [12], any complete design procedure should ensure that

- the bearings will safely support the maximum gravity service loads throughout the life of the structure
- the bearings will provide a period shift and hysteric damping during one or more design earthquakes.

The performance of the bearings as designed is evaluated under dead, live, and earthquake loads and any other load conditions that may apply.

However, the long high amplitude velocity and displacement pulses may cause large base displacements of the seismic base isolator, while buckling or rupturing isolation devices under near-fault ground motion Providakis [13]. Therefore, the stability of the base isolation system in service and seismic loading at fault-distance in the near-field region are crucial for the design of LRB-based base isolation systems [14].

Therefore, the devices of isolation system should be checked for stability and shear strain to perform a reliable design, using the assessment of global seismic response not only at *DBE* level but also and more importantly at *MCE* level. In this study, *3D* nonlinear seismic analyses of both base-fixed and associated base isolated models of a *3D* multi-story building with bearings of LRB type are performed for three near-field ground motions recorded at each of three stations with different closest distances to the active seismic fault during the 1994 *6.7 M_w* Northridge earthquake to examine the seismic performance and the effectiveness of base isolation systems designed as per *UBC97*.

Furthermore, we discuss important issues regarding the analysis and design of base-isolated buildings under near-field ground motions at both *DBE* and *MCE* levels. In addition, the numerical performance of two analyses methods to solve the *3D* nonlinear dynamic equations of motion of the studied multistorey structural models is investigated using the Newmark's and Fast Nonlinear Analysis (*FNA*) algorithms. Finally, conclusions and recommendations of engineering significance are developed to perform reliable and efficient analyses and design of nonlinear base isolation systems at both *DBE* and *MCE* levels.

2. Building structure example and seismic design parameters

2.1. Building structure example

The subject 5-story frame building has a regular plan and an elevation of 15×8 m^2 with three spans in the longitudinal direction and two spans in the transverse direction, as shown in Figure 1.
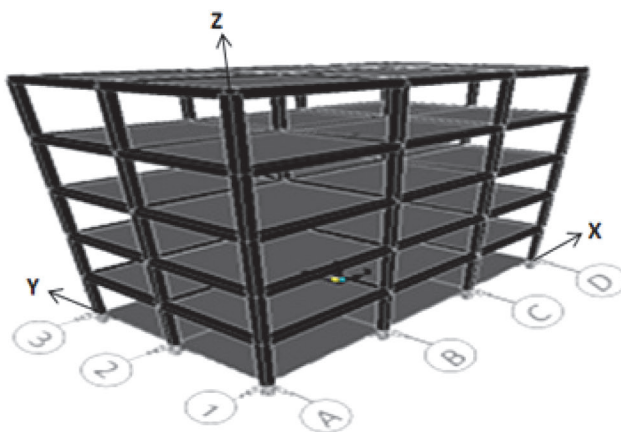
Figure 1. 3-D frame building example

Sections of the beams are 40×30 cm^2, 30×30 cm² for all columns, and a floor height of 3 m. The bearings are incorporated in between the foundation and superstructure. The superstructure is placed on an isolation system consisting of LRBs placed under each column and connected to a rigid base slab of 10 cm. The arrangement of the isolators is also shown

Table 1. Earthquake components characteristics used for 3-D nonlinear dynamic analysis and design of LRB isolator

Seismic event	Station	Closest distance [km]	Component	PGA [g]	PGV [cm/s]	PGD [cm]
17- 01-1994, 6.7 M_w Northridge earthquake	Pardee	**5.54**	NORTHR_PAR-L NORTHR_PAR-T NORTHR_PAR-UP	0.55 0.3 0.38	76.03 54 11.10	14.43 11.06 0.48
	Canyon	**11.39**	NORTHR_LOS270 NORTHR_LOS000 NORTHR_LOS-UP	0.471 0.403 0.303	41.106 44.361 18.531	14.56 11.26 5.34
	Hollywood	**17.82**	NORTHR_WIL180 NORTHR_WIL090 NORTHR_WIL-UP	0.25 0.135 0.151	27.018 12.737 11.695	5.46 4.85 3.98

in the same figure. The total weight of the building is 7510 kN. The elasticity modulus of each frame element is 2.48x10⁷ kN/m². The natural period of vibration for the fixed-base building along the principal direction X (Obtained using SAP2000 program) is T_x=1.03 s. The superstructure modal damping ratios are assumed to be constant for each mode as 5 %. It is built on soil profile type corresponding to stiff soil profile S_D and is located in the area within seismic zone 4 (Factor, Z=0.4 as given in the table I), where the active faults capable of producing large magnitude events have a high rate of seismic activity (Class A seismic source according to Table *16-U of the UBC97*).

2.2. Near ground motion characteristics

Three ground motion components recorded at each of the three stations with different closest distances to the seismic fault of approximately 5.54, 11.39 and 17.822 km during the 1994 6.7 Mw Northridge earthquake are used to assess the effectiveness
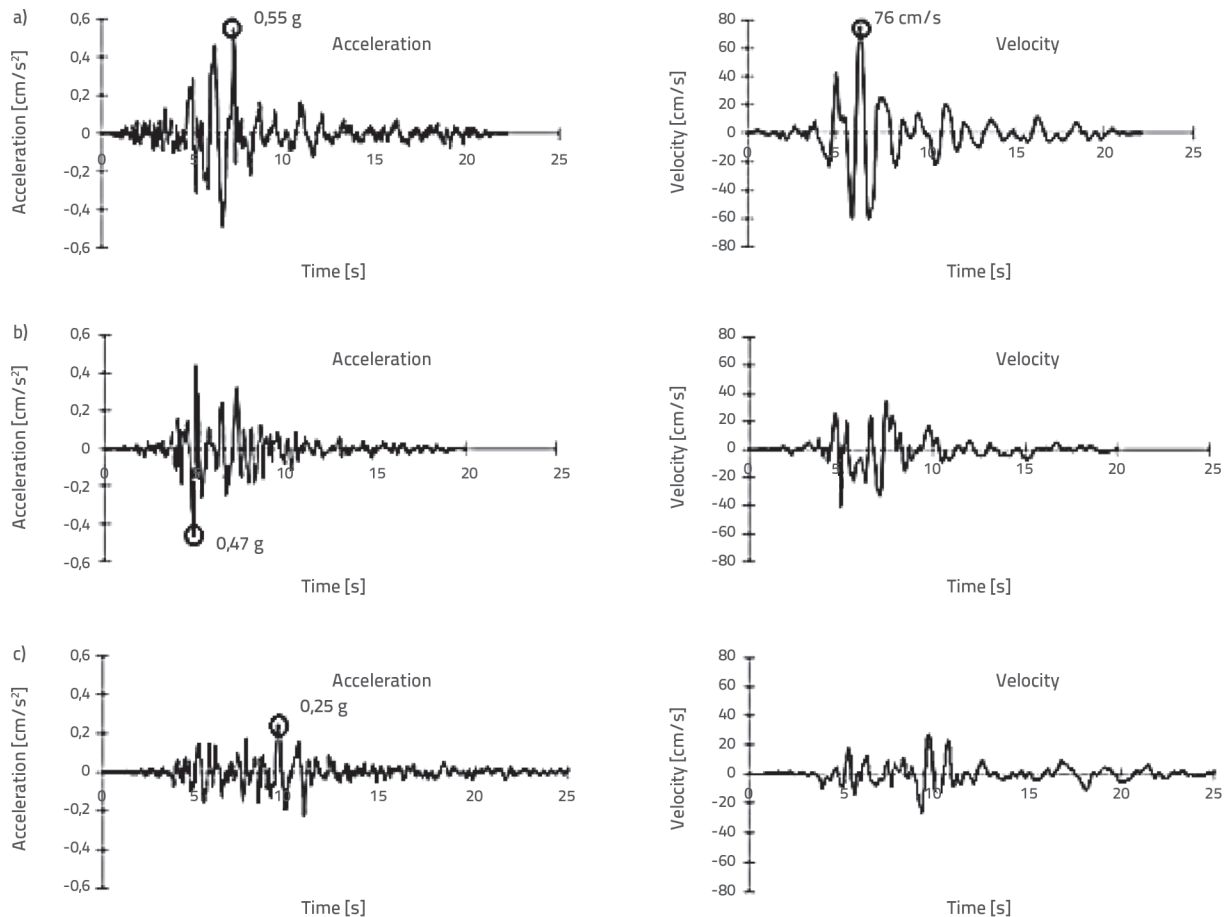
Figure 2. Near field acceleration, and velocity time history of longitudinal ground motion components recorded at Pardee, Canyon, and Hollywood stations during the 1994, 6.7 Mw Northridge earthquake

of isolation systems with LRBs. The longitudinal, transversal, and vertical components of seismic ground motions recorded at each of the three stations are simultaneously applied in the principal X, Y, and Z directions of the structure. In this study, we only present the results in X direction. Table 1 shows the characteristics of the three ground motion components recorded at each of the three stations used for isolator design. The acceleration and velocity of longitudinal ground motion components are plotted in Figure 2. There is a significant velocity pulse of 76 cm/s in the longitudinal ground motion component recorded at the Pardee station. Moreover, no significant velocity pulses in the longitudinal ground motion components were recorded at the Canyon and Hollywood stations. The peak accelerations for the longitudinal ground motion components recorded at the Pardee, Canyon, and Hollywood stations are 0.55, 0.47, and 0.25 g, respectively.

3. Isolator design procedures

3.1 Displacement criteria

Only one type of LRB is used at the base for outer and inner columns bases. The LRB isolation system should provide effective period T_D of the isolated structure (estimated to be T_D = 2.00 s), greater than three times the elastic fixed-base period T_{code} [Tcode = $c_t(h_n)^{3/4}$ = 0.072(15)$^{3/4}$ = 0.55.sec] of the structure calculated by *UBC97* formula 30-8 (i.e T_D = 2 s > 3T_{code} = 3 × 0.55 = 1.66 s). In addition, the isolation system should provide critical damping ratio of approximately 15 % (*UBC 97* formula 65-3). The design displacement of the isolation system along the main horizontal axis at Design Basis Earthquake (DBE) level is calculated using the UBC97 formula (58-1):

$$D_D = \frac{\left(\dfrac{g}{4\pi^2}\right)}{B_D} C_{VD} T_D \tag{1}$$

The seismic coefficient C_{VD} is obtained from Table 16-R of UBC97 accounting for the near-source factor N_v (C_{VD} = 0.64 N_v) obtained from Table 16-T. N_v is a near-source factor that depends on the proximity to and activity of known faults near the structure as obtained from Table 16-T of *UBC 97*.

The damping coefficient B_D =1.35 is obtained from Table A-16-C assuming damping ratio β_D = 0.15. The total design displacement, D_{TD}, of elements of the isolation system shall include additional displacement because of actual and accidental torsion, as prescribed by UBC97 formula (58-5):

$$D_{TD} = \left[1 + \frac{(12e)}{b^2 + d^2} y\right] D_D \tag{2}$$

where b and d are shortest and longest plan dimension of the structure respectively; e is the actual eccentricity (e_{actual} = 0) plus 5 % accidental eccentricity ($e_{accidental}$=8˝0.05) =0.4 m, y is the distance between the centre of rigidity of the isolation system rigidity and the element of interest, measured perpendicular to the direction of seismic loading under consideration. The value of y = 4 m is used for the elements at edges of the structure parallel to the direction of seismic loading.

3.2. Bi-linear hysteric model of isolator

The non-linear behaviour of the isolator is idealised by a bi-linear force-deformation model, which reflects the mechanical properties of bearings characterised by three main design parameters: the elastic stiffness (K_1), post-yielding stiffness (K_2), and characteristic strength (Q) [8, 15, 16]. W_D is the energy dissipation per cycle, as measured by the area enclosed by the loop of the force-deflection curve, as shown in Figure 3.
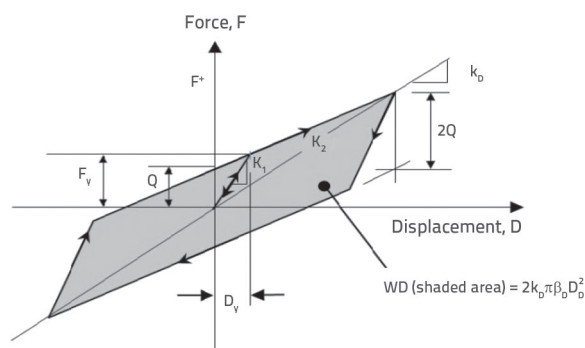
Figure 3. Bilinear model of isolator unit

Table 2. Properties of bilinear model of LRB isolator at DBE level

1994, 6.7 M$_w$ Northridge earthquake	N$_v$	C$_{VD}$	T$_D$ [s]	D$_D$ [cm]	k$_D$ [kN/m]	W$_D$	D$_y$ [m]	Q [kN]	K$_2$ [kN/m]	K$_1$ [kN/m]
Pardee Station	**1.52**	**0.977**	2	**36**	837.30	**102.03**	0	70.99	640.05	6400.5
							0.008	72.60	635.57	6355.7
							0.01225	**73.50**	**633.07**	**6330.7**
Canyon Station	**1.14**	**0.73**	2	**27**	837.30	**51.38**	0	50.33	640.12	6401.2
							0.0075	51.85	634.15	6341.5
							0.0091	**52.20**	**632.79**	**6327.9**
Hollywood Station	**1**	**0.64**	2	**24**	837.30	**39.49**	0	44.12	640.12	6401.2
							0.0055	45.23	635.15	6351.5
							0.0080	**45.77**	**632.80**	**6328.0**

The bi-linear behaviour is selected because it is applicable for most of the isolation systems used in practise. The properties of isolators for all cases of recorded near field ground motions in frame system designed according to UBC 97 are given in Table 2 after the convergence procedure of model parameters.

As shown in Table 2, the design displacement D_D increases for increasing values of the near source factor N_V and seismic coefficient C_{VD}. Furthermore, the design displacement $D_D=36\ cm$ is much larger in the Pardee station (i.e., the nearest station to the active seismic fault) than that of other stations. Additionally, the energy dissipation W_D increased substantially in the Pardee's near-fault motions indicating a strong attenuation of seismic ground motions characteristics. Therefore, considering the near-source factor is crucial.

4. Nonlinear dynamic analyses and seismic performance evaluations

In this section, we investigated the nonlinear seismic response of the *3-D* multistorey building structure (Figure 1) under three acceleration ground motion components recorded at each of three stations with different closest distances to the seismic fault during the 1994 6.7 M_w Northridge earthquake. We performed a dynamic analysis in time domain for both fixed-based and base-isolated structures. The superstructure is modelled as an elastic frame structure.

The superstructure and base are modelled with three degrees of freedom: *X, Y,* and rotational degree per floor attached to the centre of mass. The floors are infinitely rigid in plane [17]. All LRB isolation elements are connected at the base level through a rigid slab at the foundation level. The LRB bearing is modelled as LINK, in a suitable format for the SAP2000 program [18]. The SAP2000 Nonlinear finite element code is used to obtain the dynamic responses at discrete time intervals. The nonlinear direct integration (NDI) Newmark's method with parameters $\alpha = 0.5$ *and* $\beta = 0.25$ (i.e., using the unconditionally stable average acceleration method), and Fast Nonlinear Analysis (FNA) method [19] are used to integrate the

dynamic equilibrium equations of motion. The seismic performance evaluations include the top floor absolute accelerations and drifts, a maximum base displacement, and base shear. The performance criterion are defined as follows:

- Relative displacement (P_1), of the base with respect to the ground also represents the deformations of the isolators: $P_1=\max(|d_b|)$
- where d_b is the relative displacement of base with respect to the ground.
- Peak roof drift ratio (P_2) is defined as: $P_2=\max((d_s-d_b)/H)$
- where d_s is the roof relative displacement with respect to ground and H is total building height.
- Peak of the fifth floor acceleration (P_3) is defined as: $P_3=\max(|a_5|)$
- where a_5 is the total acceleration of the fifth floor.
- Peak base shear is given by: $P_4=\max(|V_b|)$, where V_b is the base shear of the structure.

The seismic performance of the base isolation systems was evaluated by comparing the dynamic responses results of the isolated building over the fixed-base building. Table 3 summarises the results demonstrating the benefits of the base isolation, along with appropriate commentaries presented in section 4.1 to 4.4. The results presented in the same table show that seismic base isolation *simultaneously* reduces seismic interstory drift and floor acceleration, contrary to the ductility base concept of reducing earthquake damages and improving structural performance for building structures. Furthermore, Table 3 shows that the FNA algorithm is more efficient than the Newmark's direct time integration method for practically the same degree of accuracy.

4.1. Base displacement response

The maximum base structural displacements in the *X* direction were found to be 14.20 cm, 4.34 cm and 2.99 for 3-D input ground motion components, respectively, recorded at Pardee, Canyon and Hollywood stations during the 1994 6.7M_w Northridge earthquake.

Table 3. Seismic performance of fixed-base and isolated buildings and numerical methods of analysis

Seismic performance evaluation	Method of analysis	Northridge Pardee record		Northridge Canyon record		Northridge Hollywood record	
		Fixed base	Isolated base	Fixed base	Isolated base	Fixed base	Isolated base
(P_1) Base displacement [cm]	NDI	0	12.92	0	2.99	0	2.07
	FNA	0	14.20	0	4.34	0	2.99
(P_2) Peak roof drift ratio [%]	NDI	3.31	1.00	0.858	0.60	0.69	0.53
	FNA	3.33	1.00	0.859	0.60	0.69	0.53
(P_3) Top-floor acceleration [m/s²]	NDI	20.13	6.61	5.50	3.10	3.90	2.49
	FNA	20.15	5.53	5.50	2.73	3.90	2.37
(P_4) Base shear [kN]	NDI	6462	1697	1624	737.8	1414	624
	FNA	6459	1791	1583	842	1421	679
CPU time [s]	NDI	464	389	211	334.48	201	260
	FNA	4	6	5	6	4	7
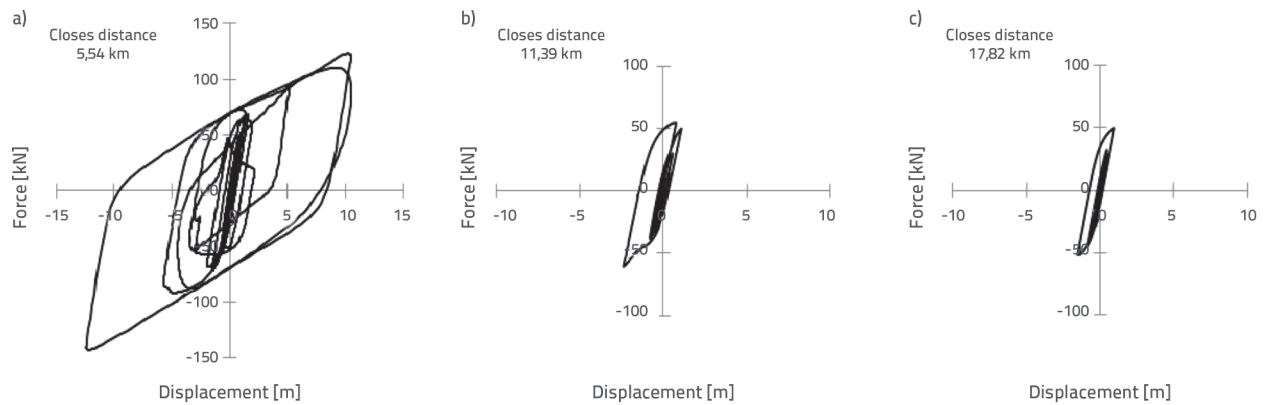
Figure 4. Force deformation curves of seismic isolator for 3-D input acceleration ground motion components recorded at: a) Pardee, b) Canyon, c) Hollywood during 1994, 6.7 M$_w$ Northridge earthquake

These are, respectively, 42 %, 17 %, and 13.5 % of the predicted design displacement calculated according to the UBC97 (see Table 2), indicating a substantial degree of conservatism in the design for the material properties and the near field ground motion characteristics selected in this study.

Figure 4 shows the typical plots of the force displacement behaviours of the isolator under three different cases of acceleration ground motions components recorded at the near field Pardee, Canyon and Hollywood stations during the 1994 6.7 M$_w$ Northridge earthquake.

The figures show that the force displacement characteristics of the isolators vary for different cases of near-field ground motion characterised by three closest distances to the seismic fault (5.54, 11.39 and 17.82 km) and corresponding PGA levels (0.55, 0.47 and 0.25g). The area of the hysteresis loop widens in the case of the ground motion input recorded at the Pardee station, i.e., the nearest station to the seismic fault. The hysteresis loops become narrow and closely spaced in the central zone for the ground motions recorded at the two farther Canyon and Hollywood stations. The computed peak displacements for all cases are less than half of the UBC97 predicted design displacements. Furthermore, seismic building codes impose a substantial degree of conservatism in the design because different earthquakes at the same location have different frequency contents and induce the different periods of the structure with varying degrees of intensity. Additionally, the bi-linear behaviour assumption made in the design stage according to the UBC97 is acceptable.

4.2. Inter-story drift displacement response

Story drift response is an important parameter for evaluating base isolation performance. The comparison of floor drifts for fixed-base and base-isolated building for the three cases of near field ground motions recorded at Pardee, Canyon, and Hollywood stations during 1994 Northridge earthquake are shown in Figures 5–7,
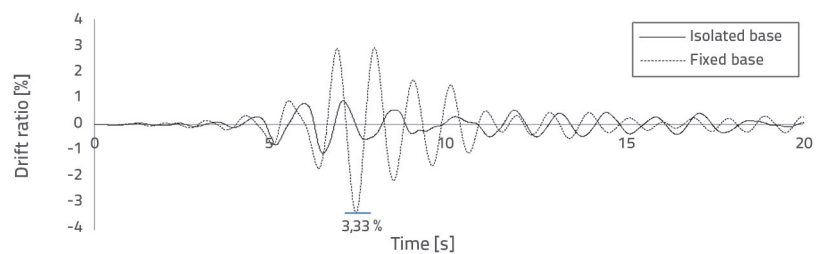
Figure 5. Drift ratio response under 1994, 6.7 Mw Northridge earthquake (Pardee station)
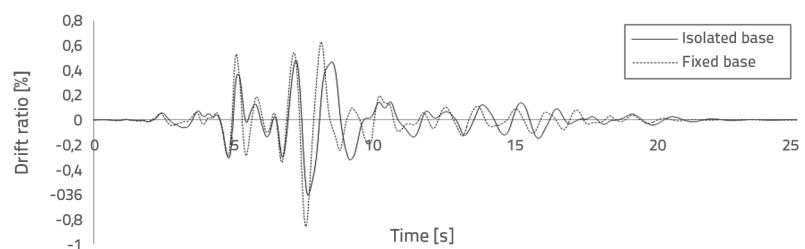
Figure 6. Drift ratio response under 1994, 6.7 M$_w$ Northridge earthquake (Canyon station)
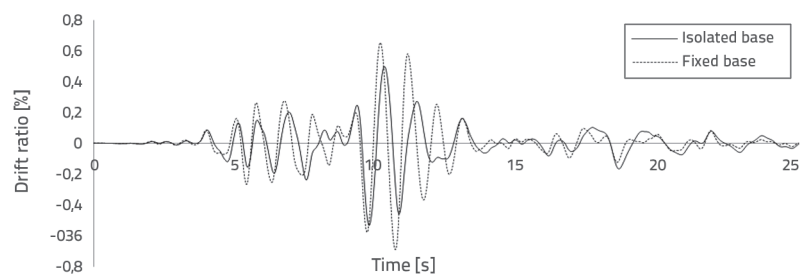
Figure 7. Drift ratio response under 1994, 6.7 M$_w$ Northridge earthquake (Hollywood station)

respectively. The story drifts of the isolated building are reduced to approximately 68 %, 30 %, and 20 % as compared to the fixed-base building in Pardee, Canyon, and Hollywood stations, respectively. Furthermore, the story drift ratio for the fixed-base building in near field ground motion recorded at the nearest station to seismic fault (Pardee station) is 3.33 %, and exceeds the maximum allowed by UBC97 (i.e., story drift should not exceed 0.020 times the story height).

4.3. Absolute acceleration response

The top floor peak absolute accelerations for the base-isolated building and the fixed-base building subjected to of near-field ground motions recorded at Pardee, Canyon, and Hollywood stations during 1994 Northridge earthquake are shown in Figure 8. The peak absolute accelerations at top floor of the base-isolated building decreases by approximately 67 %, 43 %, and 36 % of the corresponding values of the fixed-base building in Pardee, Canyon, and Hollywood stations, respectively.

	Pardee	Canyon	Hollywood
■ Fixed base	20,13	5,5	3,9
■ Isolated base	6,61	3,1	2,49
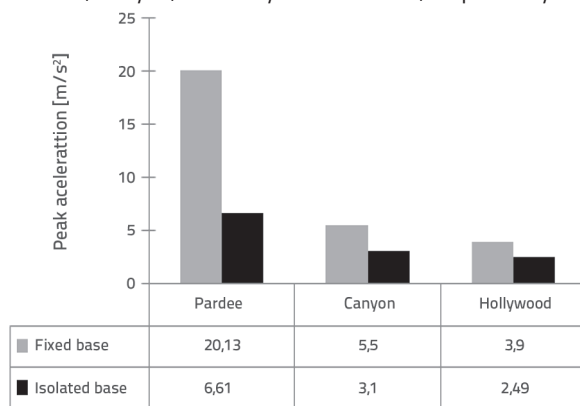
Figure 8. Top peak acceleration response

4.4. Base shear response

The *X* direction peak base shears of the isolated base and its fixed-base building for the three cases of near-field ground motions recorded at Pardee, Canyon, and Hollywood stations during the 1994 Northridge earthquake are illustrated in Figure 9.

	Pardee	Canyon	Hollywood
■ Fixed base	6462	1624	1414
■ Isolated base	1697	738	624
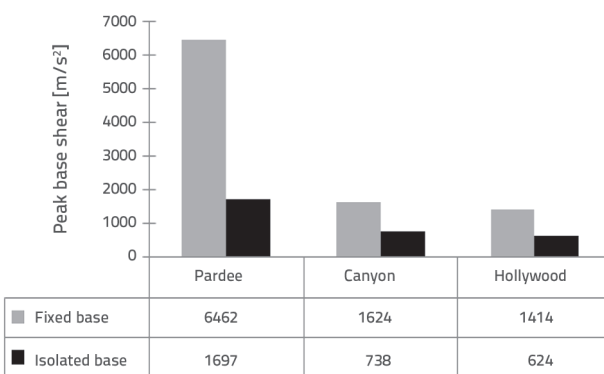
Figure 9. Base shear response

The peak base shears transmitted to the superstructure of an isolated base building are approximately 26 %, 45 %, and 44 % of their fixed-base values for the near ground motions recorded at Pardee, Canyon, and Hollywood stations, respectively. The peak base shear is reduced from $P_4 = 6462$ kN to $P_4 = 1697$ kN for near ground motion recorded at the nearest station to the seismic fault (Pardee station).

5. Geometric design, shear strain and stability checks

5.1. Preliminary geometric design

The design steps to achieve preliminary geometric design are [12, 20]:
- Choose shear modulus G ($G = 1.06$ MN/m²) and the maximum shear strain, ($\gamma_{max} = 100$ %).
- Set shape factor $S = 20$ [21]
- Calculate:
  - Total rubber thickness, $t_r = d_d / \gamma_{max}$
  - Cross-sectional area, $A = k_d t_r / G$ and ϕ the required diameter of the bearing.
  - Rubber layer thickness, t ($t = \phi / 4S$) and Number of rubber layers, ($N = t_r / t$).
  - Lead plug area; $A_p = Q / f_{py}$ ($f_{py} = 8,82$ MN/m² is yield strength of the lead plug in shear).
  - Isolator size h: $h = t_r + (N-1) t_s + 2 \times 2.5$ cm.

(Cover plates assumed 2.5 cm thick, t_s: steel plate thickness).

5.2. Shear strain and stability checks

The shear strain requirements and conditions of isolator stability checks must be satisfied at the maximum capable earthquake *(MCE)* level. Including additional displacement because of actual and accidental torsion, the total maximum displacement, D_{TM} (UBC97 formula 58-6):

$$D_{TM} = \left[1 + \frac{(12e)}{b^2 + d^2} y \right] D_M \qquad (3)$$

where

$$D_M = \frac{\left(\dfrac{g}{4\pi^2} \right)}{B_M} C_{VM} \cdot T_M \qquad (4)$$

where:
D_M - maximum displacement associated with the effective period T_M,
C_{VM} - the seismic coefficient (Table A-16-G),
N_v - the near-source factor,
B_M - the damping coefficient corresponding (Table A-16-C) and the effective period T_M at the maximum displacement D_M, assumed to be equal to 2.6 s

The rubber layers selected should satisfy under the vertical load P$_{DL+LL}$ [22]:

$$\gamma_{c,DL+LL} = \frac{6SP_{DL+LL}}{AE_c} < \frac{\zeta_b}{3} \qquad (5)$$

where $\gamma_{c,DL+LL}$ is the shear strain due to the vertical load P_{DL+LL} ($_{DL}$: dead load, $_{LL}$: live load); S is the shape factor = 20, ζ_b is elongation of rubber at break 500 % and E_c: compression modulus of the rubber-steel composite = 203365 N/cm^2

$$\sigma_c = \frac{P_{DL+LL}}{A} \leq \sigma_{cr} = \frac{GS\phi}{2.5t_r} \qquad (6)$$

To prevent the bearing from becoming unstable, the average compressive stress σ_c of the bearing should be less than a pre-set tolerance σ_{cr} [23].

Lead core size must provide the initial stiffness and energy dissipation capability to the bearing [24]:

$$1{,}25 \leq \frac{H_P}{d_p} \leq 5 \qquad (7)$$

where H_p is the effective height of the lead core, d_p is the diameter of the lead core .

Shear strain condition including the earthquake effect should be satisfied [22, 25-27]:

$$\gamma_{sc} + \gamma_{eq} + \gamma_{sr} \leq 0{,}75\zeta_b \qquad (8)$$

$$\gamma_{sc} = \frac{6SP_{DL+LL+EQ}}{E_C A_{re}} \qquad (9)$$

$$\gamma_{eq} = \frac{D_{TM}}{t_r} \qquad (10)$$

$$\gamma_{sr} = \frac{\phi^2\theta}{2tt_r} \qquad (11)$$

γ_{sc}, γ_{eq} and γ_{sr} are the shear strains under compression, earthquake, and rotation respectively.

$P_{DL+LL+EQ}$ is combination of dead load, live load, and earthquake load, A_{re} reduced cross-sectional area of bearing $\leq \phi^2(\beta-\sin\beta)/4$, where: $\beta = 2\cos^{-1}(D_M/\phi)$, and θ is rotation angle of the bearing induced by earthquake, $\theta = \left[\frac{(12e)}{(b^2+d^2)}\right]D_M$.

To avoid rollout of the bearing [22], the displacement of the bearing under the earthquake load should fulfil the following condition:

$$D_{TM} \leq \delta_{roll-out} = \frac{P_{DL+LL+EQ} \cdot \phi}{P_{DL+LL+EQ} + K_2h} \qquad (12)$$

where: d$_{roll-out}$ is the corresponding roll-out displacement.

5.3. Results for geometric design, shear stain and stability checks at MCE level

The significant effects of the near source factor on the geometric design results and corresponding dynamic characteristics of LRB isolator, and the shear strain requirements and conditions of stability checks at the MCE level are presented in Tables 4 and 5, respectively. The effects of near ground motions recorded at three stations with different closest distances to the seismic fault during the 1994 6.7 M$_W$ Northridge earthquake on the geometric design of the LRB isolator are also summarised in Figure 10.
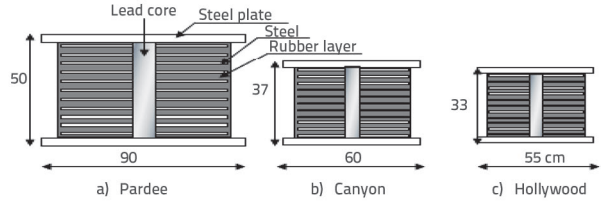
Figure 10. Designs of LRB isolator in accordance with near field ground motions recorded at Pardee, Canyon, and Hollywood stations during 1994,6.7 Mw Northridge earthquake (cm)

Furthermore, these demonstrate the importance of including the effects of closest distance parameter and torsion on the maximum total displacement at MCE level.

Table 4. Effects of near source factor on geometric design results and dynamic characteristics of LRB isolator at MCE level

1994, 6.7 M$_w$ Northridge earthquake	N$_V$*	C$_{VM}$	D$_{TM}$ [cm]	Shear strain γ_{max}	Rubber thickness t$_r$ = D$_{TM}$/γ_{max} [cm]	Diameter of bearing, $\varnothing$ [cm]	Total of height isolator, h [cm]	Lead plug area, A$_P$ [cm^2]	Effective horizontal stiffnesst, k$_D$ [kN/m]	Effective period, T$_D$ [s]
Pardee station	1.52	1.17	60	100 %	35	90	50	79	1872	1.33
Canyon station	1.14	0.89	45	100 %	26	60	37	55	1113	1.73
Hollywood station	1	0.80	41	100 %	22	55	33	51	1067	1.77
*Calculated based on the linear interpolation (See table 16-T UBC 97)										

Table 5. Shear strain and stability checks at MCE level

1994, 6.7 M_w Northridge earthquake	(1) Shear strain condition $\gamma_{cDL+LL} < \dfrac{\zeta_b}{3}$ izraz (5)	(2) Stability condition $\sigma_c \leq \sigma_{cr}$		(3) Lead core size condition $\dfrac{H_P}{dp} \leq 5$ Eq. (7)	(4) Shear strain condition for the earthquake load $\leq 0.75\zeta_b$ Eq. (8)	(5) Rollout condition $D \leq \delta_{roll-out}$ [m] Eq. (12)
		σ_c [MPa]	σ_{cr} [MPa]			
Pardee station	0.15 < 1.67	2.52	14.50	3.80<5	2.25 < 3.75	0.60 < 0.64
Canyon station	0.17 < 1.67	3.51	16.08	3.22<5	2.26 < 3.75	0.45 < 0.49
Hollywood station	0.21 < 1.67	4.24	16.86	3.01<5	2.32 < 3.75	0.41 < 0.45

Table 4 shows that for the near field ground motion recorded at Pardee station, large values of diameter, height, and horizontal effective stiffness of the isolator (hence small effective period) are observed, making it difficult to achieve the desired isolation efficiency. Furthermore, Table 5 shows that, while there is a significant degree of conservatism in shear strain and stability conditions, achieving a safety margin against the rollout condition is difficult ($D_{TM} \approx \delta_{roll-out}$)

In such a case, supplemental damping or other isolation strategies based on appropriate combinations of LRBs with other types of isolators (such as viscous fluid dampers, High Damping Rubber Bearings**,** etc.) can be used to improve the desired efficiency of base isolation (e.g.: [13, 28]).

6. Supplemental viscous dampers:

In this study, 12 supplemental nonlinear fluid viscous dampers *NFVD* have been inserted in parallel with LRB isolators along the principal X and Y directions of the building to improve the desired efficiency of base isolation and to limit the large isolator displacements at MCE level. The behaviour of a nonlinear fluid viscous damper is idealised as a pure dashpot, as shown in the constitutive equation (13) [29, 30]:

$$F_D = C_{NFVD} \times V^\alpha \tag{13}$$

Equation (14) provides the relationship between the damper output force and velocity, where C_{NFVD} and α (alpha) are the damping constant and velocity exponent, respectively. A value

of alpha equal to 1.0 represents linear dampers, whereas values other than 1.0 indicate nonlinear dampers. Specifications for alpha typically range from 0.3 to 1.0; the lower the exponent the more efficient the viscous damping for seismic energy dissipation. The supplemental damping coefficient C_{NFVD} can be calculated based on the total stiffness K=12ˇ932=11184 kN/m (each one of isolator designed gives 932 kN/m in the case of ground motion recorded at Pardee station) and total weight W=7510 kN as follows:

$$C_{NFVD} = 2\zeta_{NFVD} wm = 2\zeta_{NFVD} \sqrt{km} \tag{14}$$

Furthermore, two different values of supplemental dampinga ζ_{NFVD} = 15 % and ζ_{NFVD} = 20 %.

In the principal direction X:
- for a supplemental damping ζ_{NFVD} = 20 %

$$12 \, C_{NFVD} = 2\zeta_{NFVD} \sqrt{km} = 2 \cdot 0{,}2\sqrt{11184x751}$$

$$C_{NFVD} = 96$$

Similar calculation can be used for the principal direction *Y* of building.

The geometric design results after the addition of the supplemental damping alongside the isolators demonstrate the important role of supplemental damping played in reducing the total maximum displacement D_{TM} so that a larger B_M reduces D_{TM}, allowing a bearing with smaller diameter to be used (See Table 6). Additionally, in case of near ground motion recorded at the nearest station to seismic fault (Pardee station), the addition of the supplemental damping

Table 6. Effects of supplemental damping on geometric design results and dynamic characteristics of LRB isolator at MCE level (ζ_{NFVD} = 20 %)

1994, 6.7 M_w Northridge earthquake	Pardee record 5.54 km		Canyon record 11.39 km		Hollywood record 17.82 km	
	Without NFVD	ζ_{NFVD} 20 %	Without NFVD	ζ_{NFVD} 20 %	Without NFVD	ζ_{NFVD} 20 %
C_{VM}	**1.17**	**1.17**	0.89	0.89	0.8	0.8
B_M	**1.35**	**1.8**	1.35	1.8	1.35	1.8
D_{TM} [cm]	**60**	**45**	45	34	41	31
Diameter of bearing, $\varnothing$ [cm]	**90**	**55**	60	44	55	41
Total of height isolator, h [cm]	**50**	**37**	37	30	33	26
Effective period, T_D [s]	**1.3**	**1.89**	1.69	1.99	1.73	2

Table 7. Effects of supplemental damping on superstructure response at MCE level (ζ_{NFVD} = 20 %)

Seismic performance evaluation	1994, 6.7 Mw Northridge earthquake					
	Pardee record		Canyon record		Hollywood record	
	Without NFVD	ζ_{FVD} (20 %)	Without NFVD	ζ_{FVD} (20 %)	Without NFVD	ζ_{FVD} (20 %)
Base displacement [cm]	9.54	5.65	3.71	2.13	2	1.86
Peak roof drift ratio [%]	1.33	1.08	0.56	0.43	0.55	0.4
Base shear [kN]	2607	2244	1000	817	825	741

by the amount of 20 % increased the factor B_M from 1.35 to 1.8, reduced total maximum displacement D_{TM} from 60 cm to 45 cm and allowed the bearing diameter to be reduced to 60 cm, while improving structural performance.

Similarly, supplemental damping reduces superstructure response for the case of the near field ground motions with the smallest closest distance to the seismic source. The Pardee station in Table 7 shows that additional supplemental damping with amount of 20 % reduces the peak values of base displacement Peak, roof drift ratio and base shear by up to 40 %, 19 %, and 13 %, respectively as compared to corresponding values in the absence of supplemental damping.

7. Conclusion

3-D nonlinear seismic analyses of both base-fixed and associated base-isolated models of a 3-D multi-story building are performed for three near ground motion components recorded at each of three stations with different closest distances to the seismic fault of approximately 5.54, 11.39, and 17.82 km during the 1994, 6.7 M_w Northridge earthquake to assess the effectiveness of isolation systems with LRBs. We used the Newmark's and the Fast Nonlinear Analysis methods to solve the solutions of motion equations.

The numerical results show that the energy dissipation of the isolator decreases substantially as the closest distance to the seismic source increases, indicating a strong attenuation of seismic ground motions characteristics of the total design displacement of the isolator.

Furthermore, the output results at the design basis earthquake *(DBE)* level show the efficiency of the isolator system in reducing simultaneously the seismic response in terms of floor accelerations, inter-story drifts, and base shear.

However, the inclusion of near-source effects and torsion, increases the bearing displacement of the near-field ground motions with the smallest closest distance to the seismic source to finalize the geometric design and verify the stability of the bearing under earthquake load at the maximum capable earthquake *(MCE)* level required by *UBC 97*. Therefore, although the shear strain under dead, live, and earthquake loads and stability conditions are fulfilled, it is crucial to satisfy the rollout condition requirements because of the large isolator displacement at *MCE* level caused by the long period and large amplitude velocity pulses, indicating the need to use special provisions (supplemental nonlinear fluid viscous dampers) to improve the desired efficiency of isolation.

The use of supplemental nonlinear fluid viscous dampers alongside the isolators LRB reduces superstructure response of the near-field ground motions with the smallest closest distance to the seismic source, allowing for smaller bearing diameters and improving structural performance.

Moreover, the same degree of accuracy and the Fast Nonlinear Analysis (FNA) algorithm on the numerical level far outperform the Newmark nonlinear direct integration method and are recommended for nonlinear seismic response analyses of 3-D buildings with base isolation.

REFERENCES

[1] Nagarajaiah, S., Xiaohong, S.: Response of base-isolated USC hospital building in Northridge earthquake, Journal of Structural Engineering, 126 (2000), pp. 1177–1186

[2] Pan, P., Zamfirescu, D., Nakashima, M., Nakayasu, N., Kashiwa, H.: Base-isolation design practice in Japan: Introduction to the post-Kobe approach, Journal of Earthquake Engineering, 9 (2005) 1, pp. 147–171, https://doi.org/10.1080/13632460509350537

[3] Muhsin, A.A., Risan, H.K.: Influence of near-fault characteristics on inelastic response of multi-storey building with intensity measurement analysis, GRAĐEVINAR, 73 (2021) 11, pp. 1081–1092, https://doi.org/10.14256/JCE.2898.2020

[4] Anil, K., Chintanapakdee, C.: Comparing response of SDF systems to near-fault and far-fault earthquake motions in the context of spectral regions, Earthquake Engineering and Structural Dynamics, 30 (2001) 12, pp. 1769–1789, https://doi.org/10.1002/ eqe.92

[5] Yaghmaei-Sabegh, S., Mohammad-Alizadeh, H.: Improvement of Iranian Seismic Design Code Considering the Near-Fault Effects, IJE TRANSACTIONS C, 25 (2012) 2, pp. 147–157, https://doi.org/10.5829/idosi.ije.2012.25.02c.08

[6] Deb, S.K.: Seismic base isolation: An Overview, Current Science, 87 (2004) 10, pp. 1426–1430, https://doi.org/10.1002/9780470172742

[7] Koo, G., Lee, J., Lee, H., Yoo, B.: Stability of laminated rubber bearings and its application to seismic isolation, KSME Journal, 13 (1999) 8, pp. 595–604, https://doi.org/10.1007/BF03184553

[8] UBC: Structural engineering design provisions, Proceedings of the uniform building code, International Conference of Building Officials, https://doi.org/10.1061/(ASCE) 0733-9445(2000)126:10(1177)

[9] Pan, P., Ye, L.P., Shi, W., Cao, H.Y.: Engineering practice of seismic isolation and energy dissipation structures in China, doi: org/10.1007/s11431-012-4922-6

[10] Cheng, F., Jiang, H., Lou, K.: Smart structures innovative systems for seismic response control, 1st Edition, Francis and Tylor group, Boca Raton, USA, 2008.

[11] Alhan, C., Öncü-Davas, S.: Performance Limits of Seismically isolated buildings under near-field earthquakes, Engineering Structures, 116 (2016), pp. 83–94, https://doi.org/10.1016/j.engstruct.2016.02.043

[12] Mayes, R.L., Naeim, F.: Design of Structures with Seismic Isolation, 2nd Edition, Springer, Boston, USA, 2001., https://doi.org/10.1007/978-1-4615-1693-4

[13] Providakis, C.P.: Effect of LRB isolators and supplemental viscous dampers on seismic isolated buildings under near-fault excitations, Engineering Structures, 30 (2008), pp. 1187–1198

[14] Han, X., Warn, G.P., Kasalanati, A.: Dynamic stability testing of isolation systems composed of elastomeric bearings and implications for design, Structures Congress, (2013), pp. 2140–2150, doi: org/10.1061/9780784412848.187

[15] Park, Y.J., Wen, Y.K., Ang, A.H.S.: Random vibration of hysteretic systems under bi-directional ground motions Earthquake, Engineering & Structures Dynamics, 14 (1986) 4, pp. 543–557, https://doi.org/10.1002/eqne.4290140405

[16] Mori, A., Moss, P.J., Carr, A.J., Cooke, N.: Behaviour of lead-rubber bearings, Structural Engineering and Mechanics, 6 (1998) 1, pp. 1–15

[17] Nagarajaiah, S., Reinhorn, A.M., Constantinou, MC.: Nonlinear dynamic analysis of 3D base-isolated structures, Journal of Structural Engineering, 117 (1991) 7: pp. 2035–205, https://doi.org/https://doi.org/10.1061/(ASCE)0733-9445(1991)117:7(2035)

[18] Computers and Structures: SAP2000 Static and dynamic finite element analysis of structures, https://www.academia.edu/27943857/SAP2000_Integrated_Finite_Element_Analysis_and_Design_of_Structures_BASIC_ANALYSIS_REFERENCE, 1.1.2022.

[19] Wilson, E.L.: Three-dimensional static and dynamic analysis of structures, Berkeley, CA, Computers and Structures Inc, 2002.

[20] Kelly, J.M.: Earthquake-Resistant Design with Rubber, (2nd Edition), Springer-Verlag, London, 1997., https://doi.org/10.1007/978-1-4471-0971-6

[21] Kelly, J.M.: Earthquake-Resistant Design with Rubber, Springer-Verlag, New York, 1993., https://doi.org/10.1007/978-1-4471-3359-9

[22] American Association of State Highway & Transportation Officials AASHTO: Subcommittee on Bridges, Guide Specifications for Seismic Isolation Design, 2010.

[23] Naeim, F., Kelly, J.M.: Design of seismic isolated structures: From theory to practice, (1st Edition), John Wiley and Sons, Hoboken, NJ, USA, 1999.

[24] Yang, Y., Chang, Kuo., Yau, J.: Base isolation, Earthquake Engineering Handbook, CRC Press, Washington DC, 2003.

[25] Higashino, M., Okamoto, S.: Response Control and Seismic Isolation of Building, 1st edition, Taylor and Francis, London, 2006.

[26] Buckle, I.G., Liu, H.: Critical loads of elastomeric isolators at high shear strain, Proceedings of the 3rd U.S.-Japan Workshop on Earthquake Protective Systems for Bridges, National Center for Earthquake Engineering Research, State Univ. of New York, Buffalo, NY, 1994.

[27] Buckle, I.G., Liu, H.: Experimental determination of critical loads of elastomeric isolators at high shear strain, NCEER Bull, 8 (1994) 3, pp. 1–5

[28] Ladjel, Y., Toumi, Z.M.: Comportement dynamique non-linéaire d'un pont-caisson a-symétrique: étude de diverses stratégies d'isolation parasismique, Engineer's Thesis, Ecole Nationale Polytechnique Algiers, Algeria, 2016.

[29] Constantinou, M.C., Symans, M.D.: Experimental study of seismic response of buildings with supplemental fluid dampers, The Structural Design of Tall Buildings, 2 (1993) 2, pp. 93–132, https://doi.org/10.1002/tal.4320020203

[30] Deringöl, A.H., Güneyisi, E.M.: Influence of nonlinear fluid viscous dampers in controlling the seismic response of the base-isolated buildings, Structures, 34 (2021), pp. 1923–1941, https://doi.org/10.1016/j.istruc.2021.08.106.